A numerical study on the hydrodynamic impact of device slenderness and array size in wave energy farms in realistic wave climates

Markel Penalba[a,*], Imanol Touzón[b,c], Joseba Lopez-Mendia[b], Vincenzo Nava[b]

[a] *Center for Ocean Energy Research, Maynooth University*
Maynooth, Co. Kildare, Ireland
[b] *Tecnalia Research and Innovation*
Parque Tecnologico de Bizkaia, Edificio 700
48160, Derio, Bizkaia, Spain
[c] *Department of Mechanical Engineering*
University of the Basque Country (EHU/UPV)

Abstract

The future of wave energy converters lies in the design and realization of farms comprising of several devices, given the level of actual power flow for the individual devices and because of several operational issues. Therefore, not only the hydrodynamics of individual and isolated devices should be analysed, but interactions among devices within an array must also be carefully evaluated. In this paper, the authors attempt to parameterize the behaviour of small-, medium- and large-arrays of wave energy converters, in a particular staggered configuration, at four different locations characterized by realistic wave climates. The arrays studied in the present paper consist of heaving cylinders of different slenderness ratios. It turns out that for arrays of very short inter-device distances, regardless of the cylinder and array size, interactions are strong and lead to not negligible effects of destructive interference (total power reduction compared to the sum of isolated devices). Under these conditions, the bigger the array, the stronger the interactions and the higher the loss of power. However, a range of inter-device distances, referred to as intermediate region, where the power absorption is consistent and the interaction effect appears to be positive, has

*Corresponding author
Email address: mpenalba@eeng.nuim.ie (Markel Penalba)

been found. This intermediate region is easily detectable for small arrays, but loses its ideal characteristics with the increase of the size of the array.
Keywords: Wave energy converter, wave energy array, farm layout, wave interaction, inter-device distance

1. Introduction

Since the awareness of the exhaustion of traditional energy resources and the irreversible environmental impacts from fossil fuel combustion has increased, renewable and carbon-emission-free resources have been investigated intensively, with some resources already participating in the energy mix.

In this respect, wave energy may become an important renewable resource, as shown in [1], if the existing technologies develop sufficiently. Many different concepts of wave energy converters (WECs), based on diverse working principles (e.g. heave point absorbers, oscillating wave sure converters or pitch attenuators) have been developed during the last decades, mainly focusing on individual devices. Heave point absorbers are floating bodies, whose horizontal extent is much smaller than a wavelength [2]. They absorb wave energy through their movement at the free-surface and the conversion into electrical power can be achieved through different power take-off (PTO) systems. In detail, the hydrodynamic analysis of single point absorbers is usually carried out using the well known boundary element method (BEM) theory, because of the wide availability of several commercial or open-source codes, such as WAMIT [3], AQWA [4] or NEMOH [5], the relative ease of use and its appealing computational costs.

However, due to the actual power flow and high costs derived from construction, installation and maintenance of WECs, it seems that the only viable option is to incorporate more devices into 'wave farms'. It is therefore important to understand not only the behaviour of an isolated device, but also the interactions among the devices in a farm.

Hydrodynamic interactions in WEC arrays have been studied since the 1970's, when [6] introduced the concept of point absorber for array interactions

and [7] suggested an expression for the power absorbed by a WEC array. Different semi-analytical methods have been suggested to efficiently compute the hydrodynamic interactions within WEC arrays, such as the plain-wave method or the multiple scattering method introduced by [8] and [9]. Another alternative is the direct matrix method presented by [10]. All the aforementioned methods are based on the linear theory and provide exact solutions under certain assumptions.

More recent works analyse such hydrodynamic interactions both numerically and experimentally: [11] and [12] analyse numerically the hydrodynamic interactions as a function of different inter-device distances for different array configurations, including very large separating distances of over 2000m, while [13] investigates experimentally the interactions in large arrays.Some effort has also been dedicated in methods for array layout optimisation, for example [14] or [15], which consider wave directionality and array layout, or a more recent study [16], based on the hydrodynamic model recently presented by [17], considering six different parameters to optimise the layout. [18] presents an overview of the different methods to analyse WEC arrays and a whole section is given to WEC array modelling techniques in [19].

So far, most of the work for the analysis of the interaction among devices in a wave energy array has been carried out under regular wave conditions. Nevertheless, a more detailed approach is needed in order to accurately study the hydrodynamic interactions. For this reason, there is a gradual move in the literature towards studying such interactions in spectral seas: [20] studies cylindrical heaving bodies of different geometries in two different array configurations at the Portuguese western coast, [21] analyses absorbed power and the optimal layout including sub-optimal control in WEC arrays at the European Marine Energy Centre (EMEC), comparing results to those obtained under regular waves, and [22] studies several different configurations using the scatter-diagram information at Yeu Island in France.

The size of arrays may also be important, so large arrays have been studied in some works in the literature, such as, [23] which studies 18 *SEAREV* devices

in the array, [24] which studies 25 cylinders and 25 surging barges or [25] which studies 32 *AWS* devices.

[26] presents different factors that influence the behaviour of wave energy devices in an array, including the array configuration, the inter-device distance, the number of devices in the array and the incident direction of the wave. However, arrays of only 2-4 WECs are investigated, which may lead to incomplete and/or misleading conclusions. In addition, the geometry of the devices, particularly the slenderness ratio (radius/draft) in axisymmetric devices as shown in [20], and characteristics of the incoming waves may also influence the behaviour of the WECs in the array.

In this paper, the influence of the slenderness and the number of devices in a wave farm on the hydrodynamic performances is evaluated numerically in realistic wave climates, as function of inter-device distance. Scatter diagrams of four different locations, representative of various resource distributions, have been used in the analysis.

Section 2 introduces the hydrodynamic model used in the simulations, Section 3 describes different device geometries, the array layout configuration, array sizes and the locations, while Section 4 shows the results for each case. Finally, conclusions are drawn in Section 5.

2. Hydrodynamic model

The interaction between wave absorbers and fluid has very often been modelled by means of the linear diffraction theory, under the assumption of inviscid fluid and incompressible irrotational flow. In this study, linear theory has been considered, assuming wave and body motion amplitudes to be small with respect to the wavelength, and allowing the formulation of the solution of the boundary conditions and Bernoullis equation in terms of velocity potential and free surface displacement. The influence of nonlinear hydrostatics and Froude-Krylov forces for assessing the absorption of wave energy is still under investigation in order to define appropriate ranges of validity even if evidence of their influ-

ence on dynamics of bodies is well-known [27]. Nevertheless, the same authors suggest that the linearization of the free surface condition is consistent with the basic definition of point absorber (main dimension much smaller than the wavelength), and of course the effects are increasing with the wave amplitudes. Similarly, nonlinear radiation effects seem to be not so relevant. For all these reasons (small size of the device, small amplitudes, minor effects of nonlinear radiation), the linear theory seems to be a good choice for identifying the main characteristics of the interactions among devices, without no major impact on accuracy.

According to [28], indeed, when the bodies are large enough, the flow remains attached to the surface, and therefore, the resulting force on the body can be performed by integration of the pressures. In such cases, Froude-Krylov forces and diffraction and radiation forces can be used for the estimation of forces. When not applicable, other models for the fluid structure interactions should be used, in order to include viscous effects (for example, Morison equation, including viscous drag force, as an inertial term) or proceed to solve full Navier Stokes equations by means of Computational Fluid Dynamics (CFD), which will make the problem very cumbersome from the computational point of view.

In particular, the diffraction model can be applied either when the dimensionless Keulegan-Carpenter (KC) number is lower than a threshold value, with this threshold generally set to the value of 6, or -following an entirely equivalent interpretation- when the diffraction parameter $\pi\frac{D}{L}$ is greater than 0.5, where D is the significant dimension for the body (i.e. the diameter for a vertical cylinder) and L is the wavelength. Essentially, following [28], from mild to moderate sea states the linear diffraction model can be applied. Even in extreme sea states, viscous drag forces are negligible when the ratio $\frac{H}{D}$ is lower than 2. Therefore, for the case studies in the present paper, the drag effect is almost negligible, and only the inertial term could be taken into account for the estimation of forces, even when the Morison equation should be used.

All the above considerations yield to the conclusion that diffraction forces cover all the major effects on forces, given the occurrence matrices and scatter

diagrams in Figure 4.

Hydrodynamic coefficients are in this case obtained by using the commercial code AQWA [4]. Mesh density for the simulations has been decided after a mesh convergence study for an isolated device, where the best compromise between accuracy and computational costs was found to occur using a mesh of 2016 nodes and 504 panels. The same number of nodes and panels is used for all simulations. In such simulations, a range of 50 frequencies between 0.03 and 2 rad/s was analysed, which covers the vast majority of the exploitable ocean waves.

In the case studies, waves are modelled as 2D long-crested cylindrical waves, i.e. a unidirectional spectrum without any spreading factor is used in all the simulations, and the incoming waves are always perpendicular to the main direction of array. In undisturbed field, in general, the effects of directional spreading becomes particularly relevant in case of nonlinear waves and shallow water (see [29]). As a matter of fact, the hydrodynamic performance of the array should depend on the incident wave direction and taking into account a directional spreading function may reduce the final power output of the array especially if the devices are aligned with the mean wave direction, as noticed by [20]]. However, given the configuration of the layout of devices studied in this work and the linearity of the wave model adopted, it is reasonable to consider those effects to be of smaller entity and they have been not taken into account within the scope of this work.

2.1. Single-device

Once hydrodynamic coefficients are calculated, the equation of motion in frequency-domain is obtained from

$$-\ \omega^2(M\ +\ A(\omega))\hat{X}\ +\ j\omega(B(\omega)\ +\ B_{PTO})\hat{X}\ +\ K_H\hat{X}\ \ =\ \ \hat{F}_e(\omega) \quad (1)$$

where M is the mass, $A(\omega)$ the added-mass, $B(\omega)$ the radiation damping, $\hat{X}$ the position of the body, ω the wave frequency, K_H the hydrodynamic stiffness,

B_{PTO} the damping value of the PTO force, $\hat{F}_e(\omega)$ the excitation force and j the denotes complex number ($j = \sqrt{-1}$). Since a linear system is assumed, if sinusoidal waves are considered, motion is also a sinusoidal function that can be written as a function of time: x(t)=Re($\hat{X}e^{j\omega t}$). The same can be applied to the forces. The PTO is modelled as a linear damper and is optimised for each cylinder and sea-state. The absorbed power, $P_i(\omega)$, over one wave period is calculated as in Eq.(2) for regular waves and Eq.(4) for irregular waves [30].

$$P_i(\omega) = \frac{1}{2} B_{PTO} \omega^2 \mid \delta_i \mid^2 \tag{2}$$

where δ_i is the normalised amplitude of the oscillation in heave, $\delta_i = X/H$, being H the wave amplitude. To evaluate the power absorption under irregular waves, the energy (density) spectrum $S(\omega)$ can be defined as follows,

$$S(\omega) = \frac{1}{2} \frac{A_{sp}^2(\omega)}{d\omega} \tag{3}$$

where $A_{sp}(\omega)$ is the wave amplitude spectrum and the power absorption can be given as

$$P_{ir} = \int_0^\infty 2P_i(\omega) S(\omega) d\omega \tag{4}$$

For irregular waves, it is interesting to analyse the annual mean power, calculated by using the wave data statistics for a given location as a function of the significant wave height (H_s) and peak period (T_p),

$$\langle P_i \rangle = \sum_{(H_s, T_p)} P_{ir} C(H_s, T_p) \tag{5}$$

where $C(H_s, T_p)$ is the occurrence of each peak period and significant height in the corresponding location. The same method suggested in the present paper has been used in different studies in the literature to evaluate the power absorption of WEC arrays in irregular waves [11, 20]. However, this methodology is not unique in the literature. For example, [31] suggests a different procedure to evaluate power absorption under irregular waves including wave directionality.

2.2. Array of several devices

For the case of N devices in an array, Eq. (1) can be easily extended by introducing matrix notation

$$-(\widetilde{M}+\widetilde{A}(\omega))\omega^2\hat{X}+(\widetilde{B}(\omega)+\widetilde{B}_{PTO}(\omega))j\omega\hat{X}+\widetilde{K}_H\hat{X}=\widetilde{F}_e(\omega) \qquad (6)$$

where $\widetilde{A}$ and $\widetilde{B}$ are NxN symmetric matrices (N being the number of devices in the array, as a single degree of freedom is considered for each device), $\widetilde{M}$ and $\widetilde{K}_H$ are diagonal matrices of the same order as $\widetilde{A}$ and $\widetilde{B}$, and $\hat{X}$ and $\widetilde{F}_e$ are Nx1 vectors. Matrices $\widetilde{A}$ and $\widetilde{B}$ are symmetric because cross values represent hydrodynamic interaction studied in pairs, where the effect of the device i on the device j and vice versa are the same ($a_{ij}=a_{ji}$).

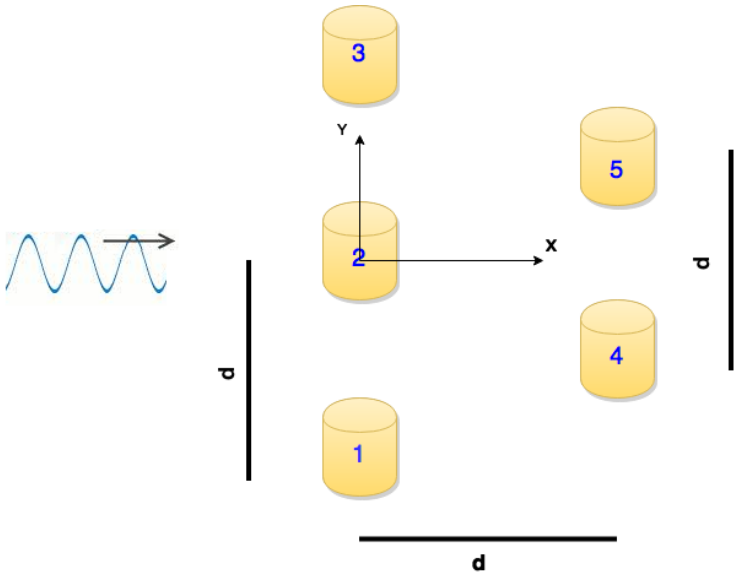

Figure 1: Staggered configuration of the 5 device array

Figure 1 illustrates the case of an array with 5 devices. Hydrodynamic coefficients obtained with the AQWA code for the case of an isolated device and the case with 5 devices are shown in Figure 2. Cylinders of slenderness

ratio ($radius/draft$) equal to 1 are used in both isolated and 5-device array shown in Figure 2, where the inter-device spacing in the array is of 5 diameters (d=5D∼125m, where D is the diameter of the cylinder). Figure 2 shows that terms of the main diagonal in the matrix are similar to the coefficients of the isolated case, except for the small fluctuations, which appear due to the interaction in the array.

The symmetry of the layout configuration illustrated in Figure 1, makes the coefficients to be symmetric with respect to the y axis (1=3 & 4=5). Therefore, hydrodynamic coefficients for the devices 1 and 3, and 4 and 5 in the array are identical, as shown in Figure 2.

Time average absorbed power by the array of N devices is calculated as follows in regular waves,

$$P_{array}(\omega) = \frac{1}{2}\omega^2 Re(\hat{\delta}_i * \widetilde{B}_{PTO}\hat{\delta}_i) \tag{7}$$

where, $*$ expresses complex conjugate transpose between $\widetilde{B}_{PTO}$, a diagonal matrix, and $\hat{\delta}_i$, a Nx1 vector.

Power absorption of arrays subject to irregular waves is calculated in the same way as for single-devices following Equations (4) and (5), where the absorbed power (P_i) in Equation (4) is given by Equation (7). All the hydrodynamic coefficients are obtained by means of the Ansys AQWA software, accounting for the mutual interactions within the array.

In this case, the PTO coefficient (B_{PTO}) is the same for all the devices in the array, as [20] reported no significant improvement is obtained by individually optimising the PTO coefficient of each device. So $\widetilde{B}_{PTO}$ diagonal matrix can be replaced by the corresponding B_{PTO} value for the isolated device and an identity matrix (I) of the adequate order. The B_{PTO} coefficient is optimized for each sea-state and cylinder type, as in the case with a single device.

2.2.1. Gain factor (q)

In the case of WEC arrays, the gain- or q-factor allows for the study of absorbed power variations in percentage terms, between that for an isolated

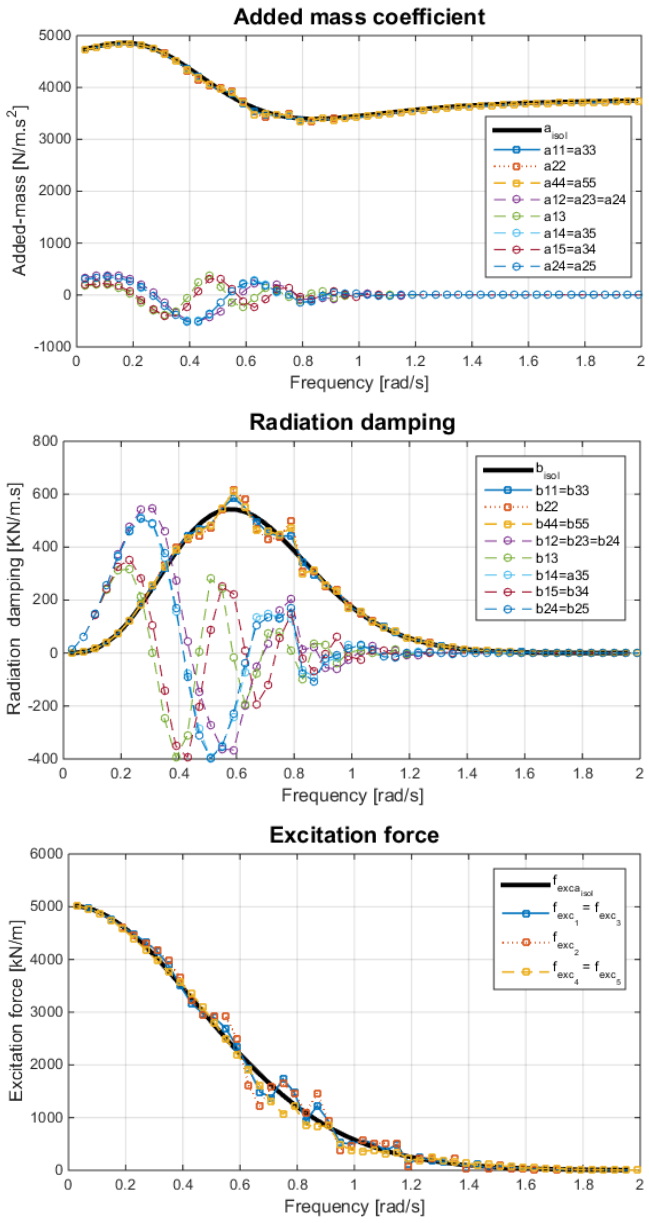

Figure 2: Hydrodynamic coefficients for a 5-device array comprises cylinders of ratio equal to 1 and inter-device spacing of 5 diameters, compared to the isolated case: added-mass (top), radiation damping (middle) and absolute value of the excitation force (bottom)

device ($P_{isolated}$) and those in an array (P_{array}) as follows,

$$q = \frac{P_{array}}{NP_{isolated}} \tag{8}$$

where, N is the number of devices, P_{array} is the total time-averaged absorbed power by the array and $P_{isolated}$ is the time-averaged absorbed power by the isolated device.

That way, the q-factor allows for comparison between the performance of arrays of different number of devices. This concept was first introduced by [6] and [7] in the late 1970's when analysing WEC arrays and has been used by several studies, such as [11] or [20], and provides a simple measure of the effect of hydrodynamic interactions in a WEC array in terms of power absorption.

When $q > 1$, power absorption of the whole array is bigger than the power absorption of an isolated device multiplied by the number of devices of the array. Thus, the interaction among the devices has positive effects and is known as *constructive*. In the opposite case, when $q < 1$, the interactions are negative and known as *destructive*.

Although it is possible to achieve constructive interaction theoretically under determined assumptions, it seems not to be realistic with real sea-states, due to different limitations and other aspects neglected in the theoretical analysis (such as nonlinear viscous multi-directional waves, nonlinear computation of hydrodynamic forces, realistic PTO models or realistic control strategies). That is why some authors [32] suggest that the goal of layout optimisation should be to minimize the destructive interaction.

3. Numerical examples

3.1. Device Geometry

A vertical cylinder oscillating in heave has been chosen to represent the WEC geometry, in order to simplify the analysis, based on the dimensions of the new CETO 6 device [33]. However, in order to better analyse the behaviour of heaving cylinders in arrays, cylinders with different geometrical characteristics

(I, II and III) have been studied in the simulations, using three slenderness (radius/draft) ratios: 0.5 (I), 1 (II) and 2 (III). To avoid scale effects and allow for a fair comparison, the masses of the three types of cylinders are kept the same, constraining the dimensions of the cylinders. Table 1 provides full details of the devices.

Table 1: Geometrical characteristics of the devices

device	**Radius [m]**	**Draft [m]**	**Mass [Kg]**	T_0 **[s]**
I	10	20	$6.45{\cdot}10^6$	10.2
II	12.6	12.6	$6.45{\cdot}10^6$	8.83
III	15.9	7.9	$6.45{\cdot}10^6$	7.93

The behaviour of different cylinders is studied by analysing response amplitude operators (RAOs). Figure 3 shows the RAOs in heave of each type of cylinder with respect to wave frequency, where the maximum amplitude increases as the slenderness ratio decreases. The RAOs in Figure 3 include the effect of the power take-off. Hence, the more slender the cylinder is, the bigger its response to the waves is. However, an increase in response leads to narrower ranges of frequencies where the device responds. For all these reasons, the optimal ratio cannot be identified unequivocally at first blush.

The absorbed power of each type of cylinder is calculated by using annual mean power in irregular waves, as shown in Section 2, and results are shown in Table 2 for the locations presented in Section 3.3. The Bretschneider spectrum is used to represent conditions at all locations in order to simplify the study, as no more precise information is available about the spectral shape for each location.

Note that the cylinder III appears to the optimal one, regardless of the location and the wave characteristics, in agreement with results reported in [34].

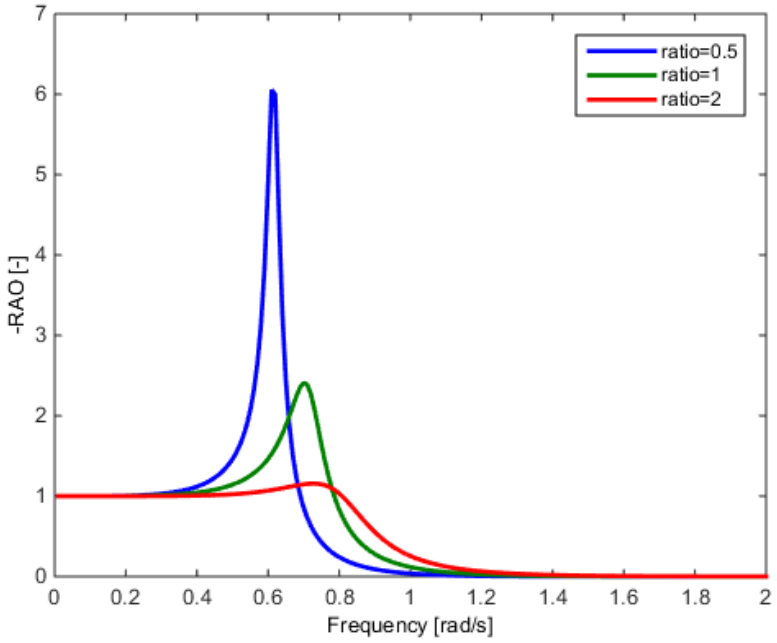

Figure 3: RAOs for the three different device geometries

Table 2: Absorbed power of isolated devices for each device type and location

	Annual mean absorbed power [kW]			
device	**Belmullet**	**Lisbon**	**BIMEP**	**SEMREV**
I	220	133	75	57
II	381	211	123	90
III	543	305	175	131

3.2. Array layout and sizes

In this paper, a single array layout is used: the staggered configuration. Devices of two consecutive rows are implemented in alternating positions, by horizontally displacing one of the two consecutive rows. That way, strong masking effects can be avoided as demonstrated numerically by [22] and experimentally by [13]. The horizontal (x) and vertical (y) inter-device spacings are identical in the arrays used in this paper. An example of such an array with 5 devices is

illustrated in Figure 1.

Regarding the size of the arrays, it seems obvious that the more devices are in the array, the stronger the interactions are, as demonstrated in [35]. However, this work only studies arrays up to 10 devices, which is considered by the authors of this paper to be a small array, since the future of wave energy devices appears to depend on farms with tens of devices, or perhaps hundreds, as mentioned by the some developers [36]. Therefore, it is interesting to analyse the effect of the hydrodynamic interactions in arrays of different number of devices, and consequently, different sizes.

In this paper, three array sizes are defined: small-, medium- and large-array. Generally, small arrays are considered those containing less than 10 devices, medium-size arrays consist of between 10 and 30 devices and large arrays include more than 30 devices, respecting the configuration illustrated in Figure 1 in all the cases. The goal of defining small, medium and large arrays is to analyse the evolution of the interaction through the different sizes. The exact number of devices used in small-, medium- and large-size arrays is 5, 18 and 39, respectively.

3.3. Locations

In order to cover a wider spectrum of the performance of wave energy devices, four different locations with different wave power resources are analysed in this study.

Table 3 shows the main characteristics of each location, while Figure 4 illustrates spectra occurrences as function of H_s and T_p, and the geographical position of each location.

T_p' and H_s' are respectively the peak period and significant height with the highest frequency of occurrence at each location and λ' is the wavelength corresponding to the peak period with the highest frequency of occurrence. J is the mean annual incoming wave energy per meter of wave front, obtained by multiplying the wave power resource (P_{wave}) of each sea-state by its statistical probability value, and summing all the sea-states of the scatter-diagram as

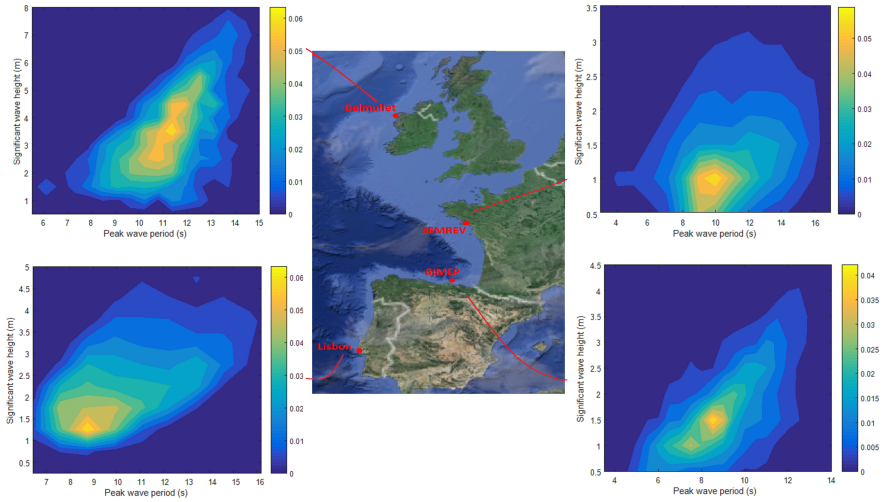

Figure 4: Different locations for the analysed arrays and their scattered diagrams

Table 3: Locations and corresponding spectral characteristics

Location	T_p' **[s]**	H_s' **[m]**	λ' **[m]**	J **[kW/m]**
Belmullet	11.3	3.5	200	78
Lisbon	8.75	1.25	120	38
BIMEP	8.5	1.5	110	22
SEMREV	10	1	160	15

follows,

$$J = \sum_{(H_s,T_p)} P_{wave}(H_s,T_p)C(H_s,T_p) \tag{9}$$

where the wave power resource of each sea-state is calculated from Equation (10) as shown in [30],

$$P_{wave} = \frac{\rho g^2 A(\omega)^2}{4\omega} \tag{10}$$

where ρ is the water density and g the acceleration due to gravity.

The selection of the test-sites is made with the aim of having as wide a representation of different wave power resources as possible.

4. Results

Results are provided in terms of the previously described q-factor, since it is the parameter that best describes the hydrodynamic interaction in arrays. Hence, the impact of slenderness and array size in wave farms is studied in different realistic wave climates as a function of inter-device distance.

Q-factor values are obtained following Equation (8), where, in the present paper, P_{array} represents the annual mean power absorbed by the array and $P_{isolated}$ the annual mean power absorbed by an isolated device, for all the different array configurations and locations. The annual mean power is obtained in all the cases using Equation (5).

Several different inter-device distances are analysed, which are normalised against the diameter of the device (D): from 2D to 60D, with an increment of 2Ds between two consecutive simulations, for small- and medium-arrays; and from 2D to 100D, with the same resolution, for large-arrays. Using normalised values, a fair comparison between devices is guaranteed.

Table 4: Power absorption and hydrodynamic interaction characteristics of 5-device arrays

	Belmullet			**Lisbon**			**BIMEP**			**SEMREV**		
device	P_{isol}	q_M	q_m	P_{isol}	q_M	q_m	P_{isol}	q_M	q_m	P_{isol}	q_M	q_m
I	1100	1.04	0.93	662	1.04	0.94	372	1.06	0.92	283	1.03	0.95
II	1907	1.03	0.95	1056	1.03	0.95	614	1.03	0.93	541	1.02	0.96
III	2715	1.05	0.95	1525	1.05	0.94	875	1.06	0.93	655	1.04	0.94

Results are divided into three main groups, analysing the behaviour of each array size separately.

4.1. Small farms

Farms of up to 10 devices are considered as small farms. In this paper, small farms are represented by arrays of 5 devices implemented in two rows, three in the front and two in the back. Figure 1 illustrates the configuration of such a small array.

Table 4 presents the main information to analyse hydrodynamic interactions in small farms, for different devices and wave climates. The variables used in the table are described as,

- P_{isol}: Power of the array in kW if all the devices of the arrays were isolated devices;
- q_M: The gain-factor value related to the inter-device distance in which power absorption is maximum; and
- q_m: The gain-factor value related to the inter-device distance in which power absorption is minimum.

The behaviour of single-devices is repeated in small arrays, where power absorption increases with the slenderness ratio. The effect of the wave climate is significant with respect to the absorbed power rate, but has practically no influence on the hydrodynamic interaction in an array. The hydrodynamic interaction is rather low in small farms, with a maximum impact of about 10% in all the cases, calculated by comparing the maximum and minimum values of the q-factor parameter in each case.

Analysing the hydrodynamic interaction in small farms as a function of the inter-device distance, the location where such interaction is maximum has been chosen: the BIMEP test site. Figure 5 shows q-factor values at each inter-device distance for the three devices defined in Section 3.1.

It is important to note in Figure 5 that markers are exact q-factor values at each inter-device distance, while lines represent the trend of the q-factor through the different inter-device distances. These trend lines are obtained by using the smoothing spline method [37], where the *R-square* parameter of the fitting is always over 0.8. The horizontal black line $q = 1$ represents the isolated case with neutral interactions or no interactions.

Hydrodynamic interactions with short inter-device distances are mostly destructive and highly inconsistent. Consequently, such short distances should be avoided. As the inter-device distance increases, hydrodynamic interactions

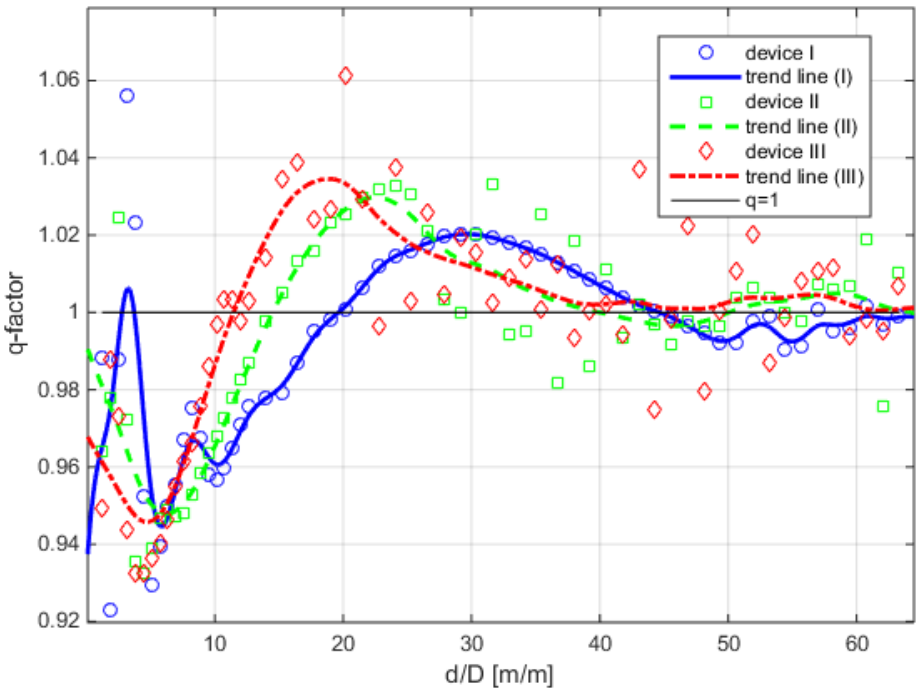

Figure 5: q-factor as function of normalised inter-device distance at BIMEP for small farms of different slenderness ratios.

become more consistent, especially for the device I, and constructive. Finally, with long inter-device distances, hydrodynamic interactions appear to vanish and devices in the farm behave as isolated devices.

Therefore, one can note three different regions with different interaction characteristics as a function of inter-device distances:

- *Short inter-device distances*: Mainly destructive and highly fluctuating hydrodynamic interactions.
- *Intermediate inter-device distances*: Constructive and relatively consistent hydrodynamic interactions.
- *Long inter-device distances*: Neutral and mostly consistent hydrodynamic interactions.

Table 5: Power absorption and hydrodynamic interaction characteristics of 18-device arrays

	Belmullet			**Lisbon**			**BIMEP**			**SEMREV**		
device	P_{isol}	q_M	q_m	P_{isol}	q_M	q_m	P_{isol}	q_M	q_m	P_{isol}	q_M	q_m
I	4523	1.05	0.85	2385	1.05	0.86	1340	1.08	0.84	1020	1.05	0.88
II	6866	1.04	0.81	3801	1.05	0.80	2209	1.07	0.77	1625	1.04	0.82
III	9778	1.06	0.73	5484	1.06	0.72	3146	1.09	0.71	2362	1.05	0.73

Trend curves clearly illustrate the three regions and highlight the differences between the three types of devices. Since constructive interaction and consistency are characteristics that WEC developers want to exploit, inter-device distances of the intermediate-region seem to be the most adequate.

The lower the slenderness ratio, the more consistent the interaction is. However, the desirable inter-device region appears to start with longer inter-device distances. In contrast, the higher the slenderness ratio is, the more constructive interactions are in the intermediate region, but the stronger the fluctuations become.

Similar trends have been presented for small arrays [22, 26, 20], paying especial attention to the constructive peaks. However, the aforementioned three regions have never been identified so far in the literature. Very little attention was paid also to the effects of the array size or the slenderness of the devices in the array, as well as realistic wave climates.

4.2. Medium farms

Arrays of 18 devices, implemented in four rows following the staggered configuration illustrated in Figure 1, are used as medium-size farms. In order to compare the impact of hydrodynamic interactions in medium farms with the impact in small farms, the situations studied in small farms are again reproduced with 18 devices: devices of three slenderness ratios and wave climate data from four different locations.

Table 5 presents the main characteristics for the study of hydrodynamic interactions in medium farms. Regarding hydrodynamic interactions, differences

between minimum and maximum q-factor values are considerably bigger for medium farms, with maximum values about 40%. The influence of the location on the behaviour of the array appears again to be irrelevant.

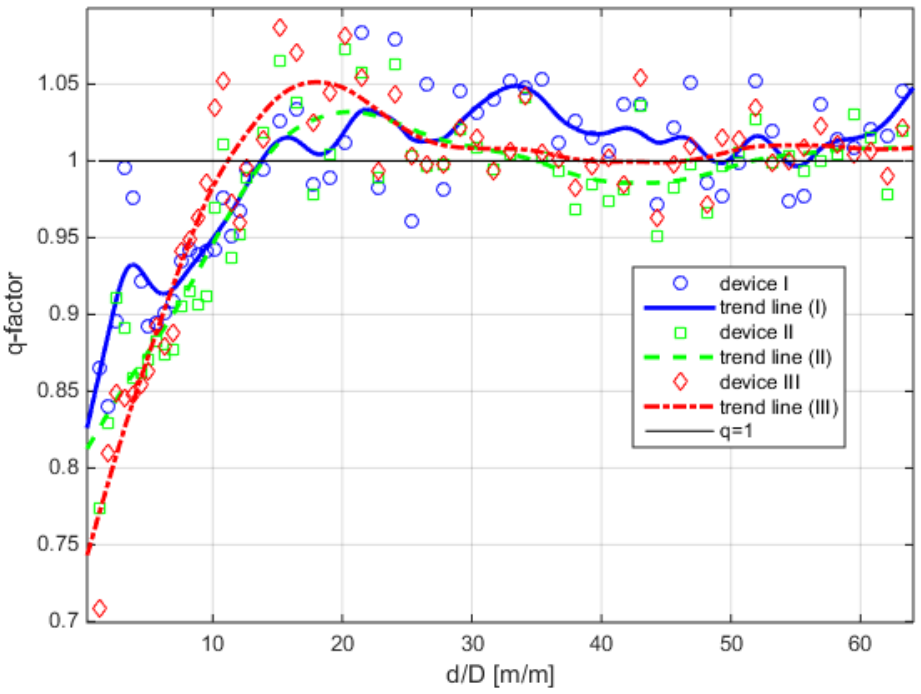

Figure 6: q-factor as function of normalised inter-device distance at BIMEP for medium farms of different slenderness ratios.

Figure 6 illustrates q-factor values for medium farms as a function of inter-device distance. In this case, fluctuations among consecutive simulations appear much stronger, rapidly moving from destructive to constructive interactions. However, trend curves still keep the desirable shape where the three regions mentioned previously in Section 4.1 are distinguishable. In contrast, the ideal characteristics of the intermediate region found in small farms, where interactions are constructive and mostly consistent, appear to weaken due to these strong fluctuations, especially in the case of the device I.

The short inter-device distances region in medium farms remains highly inconsistent and even more destructive than in small farms. The higher the

slenderness ratio, the stronger the destructive interaction is with very short inter-device distances. Nevertheless, similarly to the small farms, the intermediate region appears with shorter inter-device distances for devices with higher slenderness ratios.

4.3. Large farms

The impact of hydrodynamic interactions has been demonstrated to increase with the size of the array. However, such impact does not increase linearly with the array size, as happens with small and medium farms, but may experience a saturation-like effect with large arrays.

Therefore, an array formed by 39 devices is studied. Since the computational effort to run such a large array is extremely high, a single slenderness ratio has been chosen. Although the highest ratio permits for higher power absorption, other aspects must also be considered when designing a WEC. WEC developers tend to prefer intermediate solutions ($r = 1$), as shown in [20] or [34], so the authors consider devices of type II for the study of large arrays.

Table 6: Power absorption characteristics of 39-device arrays using only the intermediate cylinder slenderness ratio ($r = 1$).

	Belmullet			**Lisbon**			**BIMEP**			**SEMREV**		
device	P_{isol}	q_M	q_m	P_{isol}	q_M	q_m	P_{isol}	q_M	q_m	P_{isol}	q_M	q_m
II	14876	1.08	0.67	8235	1.07	0.67	4787	1.08	0.62	3521	1.06	0.68

Table 6 illustrates that hydrodynamic interactions are stronger in large arrays, with maximum values of about 50%, mainly due to stronger destructive interactions with very short inter-device distances. However, while the farm doubles the number of devices (increment of 100%), the interaction only increases 10%. Thus, a saturation-like effect has been demonstrated, as shown in Figure 7, where the impact of hydrodynamic interactions is plotted against array sizes with two increment trends for the impact of the interaction: a linear function and a quadratic function. The impact of hydrodynamic interaction in Figure 7 is referred to as the difference between the maximum and the minimum

q-factor values in percentage for each array size.

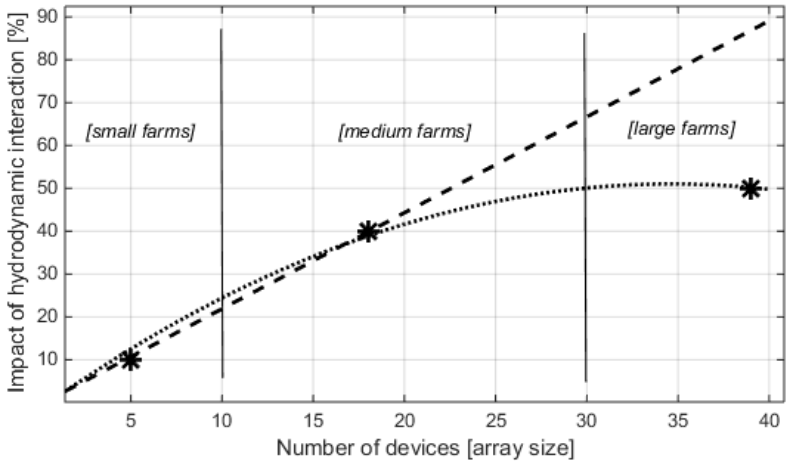

Figure 7: The impact of the hydrodynamic interaction for different array sizes.

This saturation-like effect means that after a number of devices in an array, the impact of hydrodynamic interaction may be constant, quantifiable as a constant percentage number.

With respect to the three regions identified especially in small farms, and to a lesser extent in medium farms, only the short inter-device region keeps its characteristics in large farms. The trend curve shown in Figure 8 clearly illustrates that the intermediate region completely disappears resulting in an inconsistent region where q-factor values strongly fluctuate around the neutral line ($q = 1$).

5. Conclusion

In this paper, the hydrodynamic impact of devices with different slenderness ratios and array sizes in wave energy farms is studied in four different realistic wave climates as a function of inter-device distance using the well-known q-factor.

The impact of wave climate in isolated devices is demonstrated to be important, while is practically irrelevant when studying the array configuration, since

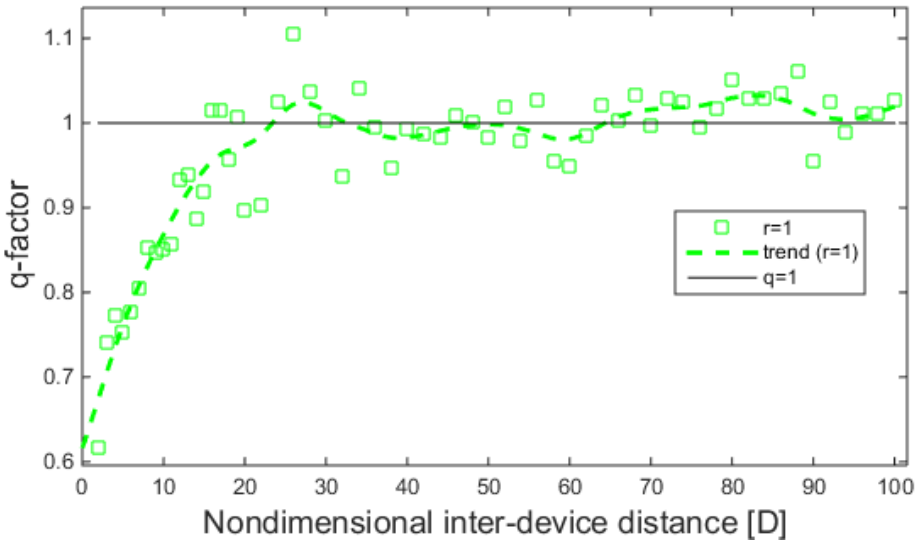

Figure 8: q-factor as function of normalised inter-device distance at BIMEP for a large farm of slenderness ratio $r = 1$

variations in q-factor values and the shape of q-factor curves are insignificant. Therefore, the design of the isolated device should be optimised for a given location, but the array configuration can be designed independently. However, the most energetic periods of all the four wave climates used in this paper are similar, so a more in-depth analysis should be carried out before the irrelevance of wave climates can be confirmed.

Analysing farms of different sizes, it is found that hydrodynamic interactions do not increase linearly with the number of devices in the array forever. Instead, hydrodynamic interactions experience a saturation-like effect which limits their impact.

In small farms, three different regions with different interaction characteristics are identified: a highly destructive and inconsistent region for short distances, a mostly constructive and consistent region for intermediate distances, and a neutral consistent region for long distances. Characteristics of the intermediate region suggest that the optimal inter-device distance in a WEC array may be found in this region. However, characteristics of such regions disappear

slowly as the size of the array increases, especially due to the intensification of fluctuations.

The slenderness of the devices implemented in the farm appears to be relevant too. Slender devices ($r < 1$) cause more consistent interactions, but longer inter-device distances are required to get constructive effects. Flat devices ($r > 1$) produce more constructive interactions with shorter inter-device distances, but fluctuations appear to be stronger. Therefore, intermediate values of slenderness ratios ($r \sim 1$) appear to be the most suitable, combining consistent and constructive effects with relatively short inter-device distances.

The deployment of arrays with smaller up to medium number of devices allows the WEC array to benefit from the ideal hydrodynamic characteristics. Ideal inter-device spacings may be between 15D and 25D for devices of intermediate slenderness ratios ($r \sim 1$). Since larger farms may be required, such large farms can be designed combining smaller arrays. Inter-array spacings should be studied to maintain the beneficial characteristics of the arrays within the farm.

Impact of wave directionality or layout configurations were not investigated in this work. Nevertheless the knowledge achieved in this study is promising towards the definition of parametric and heuristic approaches for the optimisation of array layouts based on the hydrodynamic performances of wave energy array.

Acknowledgment

This project was possible thanks to a collaboration between the University of ENSTA Bretagne in Brest (France) and the area of Marine Renewable Energy at TECNALIA. Tecnalia's authors gratefully acknowledge the support of Basque Government ELKARTEK 2015 program -grant KK-2015/00097- that made this work possible.

References

[1] G. Mork, S. Barstow, A. Kabuth, M. Pontes, Assesing the global wave energy potential, in: Procedings of 29th International Conference on Ocean, Offshore Mechanics and Artic Engineering (OMAE), China, 2010.

[2] K. Budar, J. Falnes, A resonant point absorber of ocean-wave power, Nature 256 (1975) 478.

[3] M. WAMIT Inc., WAMIT v7.0 manual (2013).

[4] A. W. ANSYS Inc., AQWA manual Release 15.0 (2013).

[5] NEMOH software (2014).
URL `https://lheea.ec-nantes.fr/doku.php/emo/nemoh/start`

[6] K. Budal, Theory for absorption of wave power by a system of interacting bodies, Journal of ship research.

[7] J. Falnes, Radiation impedance matrix and optimum power absorption for interacting oscillators in surface waves, Applied Ocean Research 2 (2) (1980) 75 – 80.

[8] P. McIver, Some hydrodynamic aspects of arrays of wave-energy devices, Applied Ocean Research 16 (2) (1994) 61–69.

[9] S. Mavrakos, P. McIver, Comparison of methods for computing hydrodynamic characteristics of arrays of wave power devices, Oceanographic Literature Review 9 (45) (1998) 1712.

[10] H. Kagemoto, D. K. Yue, Interactions among multiple three-dimensional bodies in water waves: an exact algebraic method, Journal of Fluid Mechanics 166 (1986) 189–209.

[11] A. Babarit, A impact of long separating distances on the energy production of two interacting wave energy converters, Ocean Engineering 37 (2010) 718–729.

[12] M. Göteman, J. Engström, M. Eriksson, J. Isberg, M. Leijon, Methods of reducing power fluctuations in wave energy parks, Journal of Renewable and Sustainable Energy 6 (4) (2014) 043103.

[13] V. Stratigaki, P. Troch, T. Stallard, D. Forehand, J. P. Kofoed, M. Folley, M. Benoit, A. Babarit, J. Kirkegaard, Wave basin experiments with large wave energy converter arrays to study interactions between the converters and effects on other users in the sea and the coastal area, Energies 7 (2) (2014) 701–734.

[14] B. F. M. Child, On the configuration of arrays of floating wave energy converters, Ph.D. thesis, The University of Edinburgh (2011).

[15] B. Child, V. Venugopal, Optimal configurations of wave energy device arrays, Ocean Engineering 37 (16) (2010) 1402–1417.

[16] P. M. Ruiz, F. Ferri, J. P. Kofoed, Sensitivity analysis of wec array layout parameters effect on the power performance, in: Proceedings of the 11th European Wave and Tidal Energy Conference, Nantes, 2015.

[17] J. C. McNatt, V. Venugopal, D. Forehand, A novel method for deriving the diffraction transfer matrix and its application to multi-body interactions in water waves, Ocean Engineering 94 (2015) 173–185.

[18] S. De Chowdhury, J.-R. Nader, A. M. Sanchez, A. Fleming, B. Winship, S. Illesinghe, A. Toffoli, A. Babanin, I. Penesis, R. Manasseh, A review of hydrodynamic investigations into arrays of ocean wave energy converters, arXiv preprint arXiv:1508.00866.

[19] M. Folley, Section iii - wave energy converter array modelling techniques, in: M. Folley (Ed.), Numerical Modelling of Wave Energy Converters, Academic Press, 2016, pp. 151–225. doi:http://dx.doi.org/10.1016/B978-0-12-803210-7.00010-4.
URL http://www.sciencedirect.com/science/article/pii/B9780128032107000104

[20] P. Ricci, J.-B. Saulnier, A. Falcão, Point-absorber arrays: a configuration study off the portuguese west-coast, Proceedings of 7th European Wave and Tidal Energy Conference, Porto, Portugal, September (2007) 11–13.

[21] M. Folley, T. Whittaker, The effect of sub-optimal control and the spectral wave climate on the performance of wave energy converter arrays, Applied Ocean Research 31 (4) (2009) 260–266.

[22] B. Borgarino, A. Babarit, P. Ferrant, Impact of wave interactions effects on energy absorption in large arrays of wave energy converters, Ocean engineering 47 (2012) 79–88.

[23] J. Tissandier, A. Babarit, A. Clément, et al., Study of the smoothing effect on the power production in an array of searev wave energy converters., in: The Eighteenth International Offshore and Polar Engineering Conference, International Society of Offshore and Polar Engineers, 2008.

[24] J. Singh, A. Babarit, A fast approach coupling boundary element method and plane wave approximation for wave interaction analysis in sparse arrays of wave energy converters, Ocean Engineering 85 (2014) 12–20.

[25] J. Engström, M. Eriksson, M. Göteman, J. Isberg, M. Leijon, Performance of large arrays of point absorbing direct-driven wave energy converters, Journal of Applied Physics 114 (20) (2013) 204502.

[26] A. De Andrés, R. Guanche, L. Meneses, C. Vidal, I. Losada, Factors that influence array layout on wave energy farms, Ocean Engineering 82 (2014) 32–41.

[27] H. A. Wolgamot, C. J. Fitzgerald, Nonlinear hydrodynamic and real fluid effects on wave energy converters, Proceedings of the Institution of Mechanical Engineers, Part A: Journal of Power and Energy 229 (7) (2015) 772–794.

[28] S. Chakrabarti, Handbook of Offshore Engineering, Vol. 1, Elsevier, 2005.

[29] F. Arena, A. Ascanelli, V. Nava, D. Pavone, A. Romolo, Three-dimensional nonlinear random wave groups in intermediate water depth, Coastal engineering 55 (12) (2008) 1052–1061.

[30] J. Falnes, Ocean waves and oscillating systems: linear interactions including wave-energy extraction, Cambridge university press, 2002.

[31] F. Arena, V. Laface, G. Malara, A. Romolo, A. Viviano, V. Fiamma, G. Sannino, A. Carillo, Wave climate analysis for the design of wave energy harvesters in the mediterranean sea, Renewable Energy 77 (2015) 125 – 141. doi:http://dx.doi.org/10.1016/j.renene.2014.12.002. URL //www.sciencedirect.com/science/article/pii/S0960148114008283

[32] G. Thomas, D. Evans, Arrays of three-dimensional wave-energy absorbers, Journal of Fluid Mechanics 108 (1981) 67–88.

[33] Carnegie wave energy, Available at http://www.carnegiewave.com/ (June 2016).

[34] I. Touzon, P. Ricci, M. Sanchez, G. Perez, F. Boscolo, Design, model and analysis of a combined semi-submersible floating wind turbine and wave energy point-absorber, in: In. proceedings of the 32nd International Conference on Ocean, Offshore and Arctic Engineering, Nantes, 2013.

[35] M. Vicente, A. Sarmento, Layout optimization of wave energy point absorber arrays, in: Proceedings of 10th European wave and tidal energy conference, Aalborg, 2013.

[36] Corpower ocean, Available at http://www.corpowerocean.com/ (June 2016).

[37] C. H. Reinsch, Smoothing by spline functions, Numerische mathematik 10 (3) (1967) 177–183.